CAPACITY AND DAMAGE INVESTIGATION OF PRECAST CONCRETE SELF-CENTERING SHEAR WALLS

Sina Basereh, Department of Civil, Structural, and Environmental Engineering, University at Buffalo, Buffalo, NY
Sumedh Sharma, Department of Civil, Construction, and Environmental Engineering, the University of Alabama, Tuscaloosa, AL
Paulette Baque, Department of Civil, Structural, and Environmental Engineering, University at Buffalo, Buffalo, NY
Esha Blaggan, Department of Civil, Structural, and Environmental Engineering, University at Buffalo, Buffalo, NY
Pinar Okumus, Ph.D., Department of Civil, Structural, and Environmental Engineering, University at Buffalo, Buffalo, NY
Sriram Aaleti, Ph.D., Department of Civil, Construction, and Environmental Engineering, the University of Alabama, Tuscaloosa, AL

ABSTRACT

Precast concrete shear walls with unbonded post-tensioning, which resist seismic loads have attracted the attention of researchers over the past 20 years. This study provides a database of a special subset of precast concrete shear walls tested under monotonic or cyclic loading: rocking walls, hybrid walls, and walls with end columns.

These shear walls experience joint opening, undergo rocking motion over the foundation, and utilize unbonded post-tensioning to self-center after load removal. Seismic energy is dissipated in distinct ways that vary from nonlinearity of concrete and post-tensioning strands (rocking walls) to yielding of mild steel reinforcement or external energy dissipaters (hybrid walls and walls with end columns).

The experimental drift capacity, strength, and damage sequence of walls from the literature were compiled. Onsets of cover concrete spalling, yielding of energy dissipaters, yielding of post-tensioning strands, fracture of energy dissipaters, and crushing of confined concrete were reported. ACI guidance on shear walls were evaluated by comparing the lateral drift and strength measured by testing and predicted by ACI.

Keywords: Precast shear wall, Database, Rocking, Drift capacity, Damage sequence, Residual drift

INTRODUCTION

The Precast Seismic Structural System (PRESSS) program introduced jointed precast concrete panels as an alternative to cast-in-place, monolithic, conventional reinforced concrete shear walls. In this system, individual precast panels were connected horizontally to each other through U-shaped plates along the vertical joint between the walls and anchored to the foundation using unbonded post-tensioned strands[1]. Since the PRESSS study, various types of precast concrete shear walls, with or without energy dissipation mechanisms, were investigated as seismic load resisting elements in buildings. Test data available through these studies can be used to better understand such precast concrete wall system behavior, design, and analysis methods. For this purpose, this paper compiles an experimental database of precast concrete shear walls and evaluates current design guidance[2] on wall behavior using the database.

Three types of precast concrete shear walls were considered in compiling the experimental database. 1) Unbonded post-tensioned or rocking shear walls (called rocking shear walls hereafter) refer to those in which rigid body rotation is the governing mechanism and the hysteretic response is idealized as elastic-nonlinear with relatively low energy dissipation[3-6]. The low energy dissipation stems from the nonlinear behavior of concrete and/or post-tensioning strands. 2) Hybrid rocking (or hybrid) shear walls are a combination of rocking walls and an energy dissipation mechanism. Energy dissipation is provided by yielding of conventional reinforcing bars[7-10], dog-bone-shaped mild reinforcing bars[11], and U- or O-shaped plates[1, 12-14]. 3) Precast walls with two end columns (abbreviated to PreWEC) were introduced by Aaleti and Sritharan (2007)[15] to address the lower strength of jointed wall systems. Energy dissipation is provided by O-shaped plates used between the precast wall and end columns.

One significant advantage of all three types of precast concrete walls is to minimize the damage that was observed in conventional cast-in-place walls after past earthquakes. Residual displacement can be used as a damage indicator and is expected to be much smaller in rocking, hybrid, and PreWEC walls due to self-centering provided by unbonded post-tensioning. Low residual displacements lead to a bilinear or flag-shaped hysteretic load-displacement relationship. The behavior of rocking walls can be characterized into the following limit states: decompression (initiation of gap opening), effective linear limit (initiation of significant softening), cover spalling, yielding of post-tensioning strands, and crushing of confined concrete[3]. In addition to these, hybrid and PreWEC walls may experience yielding and fracture of energy dissipaters.

Design and analysis of precast concrete walls are documented by the ACI ITG-5.2-09[2]. In this paper, the guidance of ACI ITG-5.2-09 on strength, drift capacity, residual displacements, plastic hinge length was evaluated using the database that stores information on geometric and material properties, loading condition, strength, drift capacity, and damage sequence of precast walls. The strength and drift capacity of the walls were calculated using ACI ITG provisions and compared with the experimentally reported values. ACI ITG requirements to achieve self-centering in the form of low residual drift were evaluated. The plastic hinge height data obtained from the experimental data were compared with the one predicted by the ACI ITG provisions and other resources in the literature. Finally, drift ratios at which given limit states were observed were documented. Figure 1 shows the schematic representation of rocking, hybrid, and PreWEC walls.

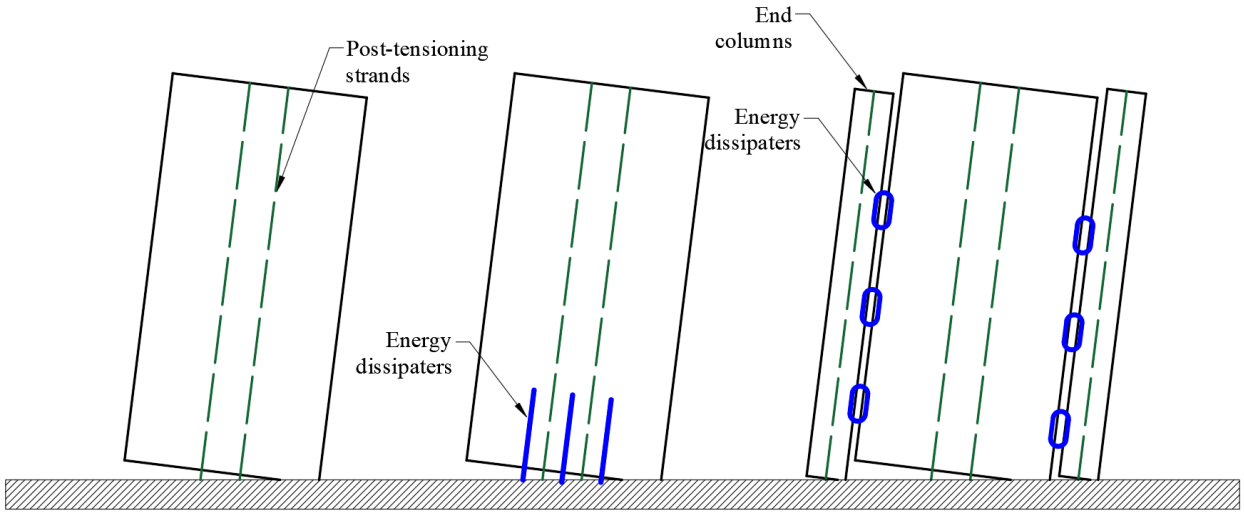

Figure 1. Schematic representation of rocking, hybrid, and PreWEC walls

DATABASE

The database consists of three precast shear wall types: 38 rocking, 7 hybrid, and 4 PreWEC walls tested under quasi-static monotonic or quasi-static cyclic loading. Aspect ratios (i.e., height-to-length ratios) of the shear walls in the database ranged from 1.5 to 3.6. The compressive strength of concrete in the database varied from 3.74 to 11.23 ksi. Conventional or dog-bone-shaped mild reinforcement was used for hybrid walls, while O-connectors were utilized for PreWEC systems. All studies, except for one on rocking walls[6], used walls with confined concrete. Table 1 provides details on the geometric and material properties of walls in the database along with the amount of axial load imposed by either gravity or post-tensioning.

Table 1. Database of precast concrete walls with unbonded post-tensioning

	Reference	ID	Geometric properties			Material properties				Gravity load (kips)	$\frac{P+N}{A_g f_c'}$	No. of PT bundles
			H_w (in.)	L_w (in.)	t_w (in.)	f_c' (ksi)	f_{py} (ksi)	f_{yED} (ksi)	f_{uED} (ksi)			
Rocking	Perez et al. (2007)[16]	TW1	285	100	6	7.60	138	-	-	173.4	0.18	3
		TW2	285	100	6	7.60	138	-	-	173.4	0.18	3
		TW3	285	100	6	8.00	138	-	-	173.4	0.17	3
		TW4	285	100	6	8.00	138	-	-	173.4	0.11	3
		TW5	285	100	6	8.00	138	-	-	173.4	0.11	3
	Rahman and Restrepo (2000)[11]	Unit 1	146	53	2.74	5.94	208	-	-	0	0.03	2
	Henry (2011)[6]	A3	118	79	5.51	4.77	152	-	-	0	0.01	2
		A4	118	79	5.51	4.77	152	-	-	0	0.02	2
		B1	130	39	5.51	4.60	152	-	-	0	0.02	1
		B2	130	39	5.51	4.60	152	-	-	0	0.03	2
		B3	130	39	5.51	4.60	152	-	-	0	0.05	3
		B4	130	39	5.51	4.60	152	-	-	0	0.08	3
		C11	118	39	4.72	3.74	229	-	-	0	0.07	2
		C12	118	39	4.72	4.05	229	-	-	0	0.07	2

		C13	118	39	4.72	3.74	229	-	-	0	0.17	3
		C14	118	39	4.72	4.05	229	-	-	0	0.16	3
		C21	87	39	4.72	4.08	229	-	-	0	0.07	2
		C22	87	39	4.72	4.08	229	-	-	0	0.07	2
		C23	87	39	4.72	4.08	229	-	-	0	0.15	3
		C24	87	39	4.72	4.08	229	-	-	0	0.15	3
		D11	118	79	4.72	3.77	229	-	-	0	0.06	3
		D12	118	79	4.72	3.77	229	-	-	0	0.06	3
		D13	118	79	4.72	3.77	229	-	-	0	0.13	5
		D14	118	79	4.72	3.77	229	-	-	0	0.13	5
		D21	87	79	4.72	4.08	229	-	-	0	0.03	3
		D22	87	79	4.72	4.08	229	-	-	0	0.05	3
		D23	87	79	4.72	4.08	229	-	-	0	0.09	5
		D24	87	79	4.72	4.08	229	-	-	0	0.12	5
		E1	118	39	4.72	6.15	229	-	-	0	0.06	1
		E2	118	39	4.72	5.83	229	-	-	0	0.05	2
		E3	118	39	4.72	6.15	229	-	-	0	0.07	3
		E4	118	39	4.72	5.83	229	-	-	0	0.11	3
		F1	118	79	4.72	5.73	229	-	-	0	0.04	3
		F2	118	79	4.72	5.67	229	-	-	0	0.05	3
		F3	118	79	4.72	5.73	229	-	-	0	0.06	5
		F4	118	79	4.72	5.67	229	-	-	0	0.09	5
	Twigden et al. (2017)[13]	A	118	39	4.72	4.64	145	-	-	0	0.02	2
		B	113	32	4.92	5.07	223	-	-	0	0.08	3
Hybrid	Smith (2012)[7], Smith et al. (2010)[8], Smith and Kurama (2014)[17]	HW1	163	96	6.25	4.74	235	65.0	88.2	81.2	0.07	2
		HW2	163	96	6.25	6.53	235	65.0	88.2	81.2	0.05	2
		HW3	163	96	6.25	8.02	235	67.0	94.0	81.2	0.04	2
		HW4	163	96	6.25	6.95	235	67.5	96.8	81.2	0.05	2
		HW5	163	96	6.25	6.54	235	68.4	100.0	120.0	0.05	2
	Rahman and Restrepo (2000)[11]	Unit 2	146	53	2.74	6.96	208	66.7	91.4	0	0.02	2
		Unit 3	146	53	2.74	4.49	208	66.7	91.4	45.0	0.07	2
PreWEC	Twigden et al. (2017)[13]	PreWEC A	113	32	4.72	6.19	223	46.4	65.3	0	0.05	3
		PreWEC B	113	32	4.72	5.90	223	46.4	65.3	0	0.06	3
	Sritharan et al. (2015)[18]	PreWEC	240	72	6.00	9.14	243	58.0	76.3	0	0.12	1
	Liu (2016)[19]	PFS2	220	68	6.00	10.9	263	60.0	73.2	13.0	0.03	1

H_w, L_w, and t_w: Height, length, and thickness of the wall, respectively.
f_c', f_{py}: compressive strength of concrete, and yield strength of post-tensioning strands, respectively.
f_{yED}, f_{uED}: yield and tensile strength of the energy dissipater, respectively.
$\frac{P+N}{A_g f_c'}$: axial force ratio (AFR)

DRIFT CAPACITY

ACI ITG-5.2-09[2] identifies two drift limits. 1) A design drift that corresponds to the design level earthquake excitations, and 2) a maximum drift corresponding to maximum considered earthquake excitations. Unless otherwise stated, drifts reported in the database are to be compared to calculated maximum drift because experimental programs typically load specimens to failure or to the capacity of the equipment. It is worth mentioning that ACI ITG-5.2-09 simplifies the analytical calculation of drift capacity by assuming that all energy dissipaters and post-tensioning strands are placed at wall mid-length. In this study, the same assumption was made to evaluate the accuracy of the assumption for hybrid walls. For PreWEC systems, the connectors are typically placed at both ends of the wall, making the above assumption unrealistic. Thus, the actual location of energy dissipaters was considered for PreWEC systems.

To estimate the drift at failure, an estimate of plastic hinge height, strain at extreme compression fiber at the base, and the neutral axis depth at failure are needed. Plastic hinge height is the height over which the nonlinear behavior of the system is concentrated. The plastic hinge height of rocking, hybrid, and PreWEC systems is less than that of a conventional cast-in-place reinforced concrete wall due to a gap opening at the base of the wall[12]. ACI ITG 5.2-09 specifies that the plastic hinge height can be conservatively taken as 0.06 times the height of the wall, which was used in this study for estimating the plastic hinge height.

Various techniques are available to measure strain at extreme compression fiber at failure. However, since concrete strain measurements are prone to errors due to cracking and crushing of concrete at large displacement cycles, in this study, strain at extreme compression fiber was set to be the ultimate strain capacity of confined concrete calculated using the stress-strain relationship developed by Mander et al. (1988)[20]. ε_{cmax} can also be determined using Equation 1 per ACI ITG-5.2-09.

$$\varepsilon_{cmax} = 0.004 + 4.6\varepsilon_{sut}\left(\frac{f_L'}{f_{cc}'}\right) \quad (1)$$

where, ε_{sut} is the ultimate strain capacity of confining reinforcing bars, f_L' is the effective lateral stress provided by confining reinforcing bars, and f_{cc}' is the confined concrete strength.

The neutral axis depth ranged between 10 to 15 percent of the length of the walls for the walls in the database. In this study, the neutral axis depth of each wall was used as reported by the experimental studies in the database.

Having the plastic hinge height, strain at extreme compression fiber, and neutral axis depth at failure, the maximum drift capacity (θ_{Lmax}) can be determined using Equation 2 per ACI ITG-5.2-09. Additionally, section 4.3.4 of ACI ITG 5.2-09 limits the maximum drift as shown in Equation 2 as a function of wall height (h_w) and length (l_w). In this study, the minimum of the drifts calculated by Equations 2 and 3 was selected as the drift limit.

$$\theta_{Lmax} = \frac{\varepsilon_{cmax} L_p}{c} \quad (2)$$

$$0.9 \leq 0.8\left[\frac{h_w}{l_w}\right] + 0.5 \leq 3.0 \quad (3)$$

where, ε_{cmax} is the strain at the extreme compression fiber, L_p is the plastic hinge height, and c is the neutral axis depth.

Table 2 shows the measured and calculated neutral axis depth, and drift at failure. Measured and calculated maximum drift at failure did not match well. The average ratio of drift predicted by ACI and tests was 0.58 with a standard deviation of 0.39. This was likely because the analytical maximum drift is heavily dependent upon the assumptions made for the plastic hinge height and the strain at the extreme compression fiber. As shown in the next sections, there exists a high scatter for the plastic hinge height data and the assumptions made may not be accurate for all specimens.

STRENGTH

ACI ITG-5.2-09 uses the term probable flexural strength at the maximum drift. It simplifies the calculations by assuming that all energy dissipaters and post-tensioning strands are placed concentrically at mid-length of the wall, and energy dissipaters have reached their tensile strength. In this study, the same assumption was made for all walls except for the PreWEC system, in which energy dissipaters were placed at both ends of the precast wall.

The probable flexural strength is the sum of moment contributions from energy dissipaters (M_s), and post-tensioned strands (M_{prs}) as shown in Equation 4. The moment contribution of post-tensioning strands was calculated by Equation 5, which is modified from ACI ITG-5.2-09 by adding the effect of gravity load (N). The moment contribution of energy dissipaters was calculated using Equation 6 for rocking and hybrid walls as these walls typically have energy dissipation near the mid-length of the wall. For PreWEC systems, energy dissipaters are typically placed at the wall/column interface. Equation 6 was modified to Equation 7 to account for this difference and used for the PreWEC systems. The contribution of trail and lead columns was neglected for simplicity.

$$M_{pr} = M_{prs} + M_s \tag{4}$$

$$M_{prs} = \frac{(A_{ps} f_{prs} + N)(l_w - a)}{2} \tag{5}$$

$$M_s = \frac{A_s f_u (l_w - a)}{2} \tag{6}$$

$$M_s = n_{con,trail} f_{con,trail} \left(l_w - \frac{a}{2}\right) - n_{con,lead} f_{con,lead} \left(\frac{a}{2}\right) \tag{7}$$

where, $a = \beta c$, n_{con} is the number of connectors, and f_{con} is the force developed in the connectors when they are deformed. The force in the connectors was obtained from the vertical displacement measured by testing for the walls in the database and displacement-force relationship as documented by connector testing.

Peak shear force was determined by dividing the probable moment strength by the height of the wall. Table 2 exhibits measured and calculated peak shear forces. The results showed that there was a good agreement between peak shear force measured by tests and predicted by ACI ITG-5.2-09. The average ratio of shear predicted by ACI to tests was 0.88 with a standard deviation of 0.23.

Table 2. Comparison of measured and calculated drift, and strength capacity

	Reference	ID	AFR	θ_{expr}	V_{expr} (kips)	$\frac{\theta_{ACI}}{\theta_{expr}}$	$\frac{V_{ACI}}{V_{expr}}$
Rocking	Perez et al. (2007)[16]	TW1	0.18	3.50	161	0.84	1.07
		TW2	0.18	2.85	157	1.06	1.12
		TW3	0.17	2.75	154	1.09	1.14
		TW4	0.11	3.50	141	0.84	1.23
		TW5	0.11	6.00	99	0.50	1.03
	Rahman and Restrepo (2000)[11]	Unit 1	0.03	2.80	13	0.59	0.83
	Henry (2011)[6]	A3	0.01	1.20	25	0.44	0.63
		A4	0.02	1.18	28	0.32	0.73
		B1	0.02	1.82	5	0.81	0.92
		B2	0.03	1.64	12	0.55	0.62
		B3	0.05	1.63	16	0.39	0.58
		B4	0.08	1.58	18	0.32	0.65
		C11	0.07	2.61	18	0.27	0.56
		C12	0.07	2.30	14	0.40	0.80
		C13	0.17	1.91	20	0.24	0.90
		C14	0.16	1.13	20	0.33	0.87
		C21	0.07	1.40	18	0.53	0.83
		C22	0.07	1.39	18	0.40	0.75
		C23	0.15	1.15	28	0.27	0.87
		C24	0.15	0.99	30	0.31	0.82
		D11	0.06	1.32	43	0.27	0.70
		D12	0.06	1.42	46	0.29	0.68
		D13	0.13	0.82	66	0.22	0.81
		D14	0.13	0.80	70	0.31	0.84
		D21	0.03	1.33	52	0.29	0.63
		D22	0.05	0.94	48	0.27	0.83
		D23	0.09	1.04	91	0.19	0.67
		D24	0.12	0.58	87	0.22	0.83
		E1	0.06	2.67	9	0.41	1.72
		E2	0.05	2.03	16	0.33	0.62
		E3	0.07	1.82	19	0.23	0.67
		E4	0.11	1.16	22	0.38	0.84
		F1	0.04	1.18	41	0.38	0.78
		F2	0.05	1.02	48	0.44	0.86
		F3	0.06	0.96	64	0.33	0.74
		F4	0.09	0.73	73	0.29	0.77
	Twigden et al. (2017)[13]	A	0.02	1.75	9	1.71	1.47
		B	0.08	3.00	15	1.00	1.08

Hybrid	Smith (2012)[7], Smith et al. (2010)[8], Smith and Kurama (2014)[17]	HW1	0.07	1.90	119	0.56	0.87
		HW2	0.05	1.55	118	1.12	0.95
		HW3	0.04	2.30	124	0.58	0.95
		HW4	0.05	3.05	120	0.98	1.01
		HW5	0.05	1.55	142	1.94	0.90
	Rahman and Restrepo (2000)[11]	Unit 2	0.02	3.00	18	1.00	1.02
		Unit 3	0.07	4.10	27	0.73	0.98
PreWEC	Twigden et al. (2017)[13], Twigden and Henry (2015)[21]	PreWEC A	0.05	3.00	23	1.00	1.28
		PreWEC B	0.06	3.00	26	1.00	1.19
	Sritharan et al. (2015)[18]	PreWEC	0.12	3.50	114	0.86	0.94
		Minimum				0.19	0.56
		Maximum				1.94	1.72
		Average				0.58	0.88
		Standard deviation				0.39	0.23

PLASTIC HINGE HEIGHT

Plastic hinge height is critical in predicting the concrete strain demand at rocking corners. Figure 2 shows the plastic hinge height for rocking walls schematically. Several researchers provided equations for plastic hinge length of rocking walls (see Table 3).

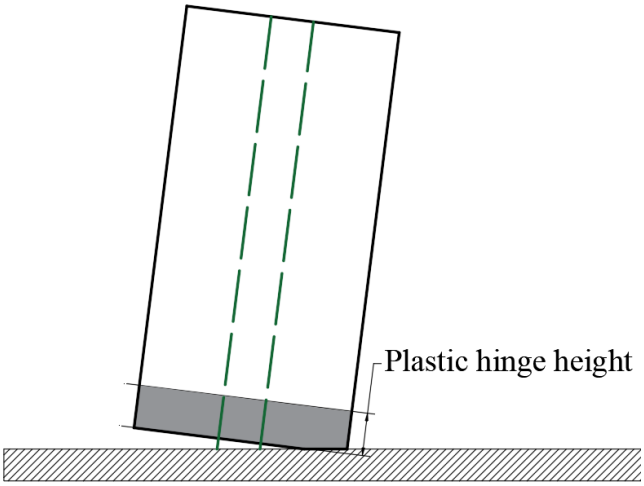

Figure 2. Plastic hinge height for rocking walls

A subset of the experimental data given in Table 1 was analyzed to evaluate the accuracy of plastic hinge height predictions proposed by different researchers. Only the test specimens with confinement at rocking corners and adequate information to process Equation 8-11 were analyzed.

Table 3. Equations for plastic hinge height

Reference	Plastic Hinge Height (L_p)	Description
Rahman and Restrepo (2000)[11]	c	c = neutral axis depth
Perez et al. (2004)[4]	t_w'', if $t_w''<2a''$ $2a''$, if $2a''<t_w''$	t_w''= wall thickness measured between confinement reinf. a''= equivalent confined concrete stress block measured from confinement reinforcement
Kurama (2005)[22]	$0.2\ L_w$	L_w=length of wall
ACI ITG (2009)[2], Aaleti and Sritharan (2009)[23]	$0.06\ h_w$	h_w= height corresponding to lateral load location

The total curvature, which is the summation of elastic and plastic curvatures, at the base of the wall (ϕ_t) for a given drift level for the experimental walls was calculated using the measured neutral axis depth (c_θ) and concrete strain value (ε_θ) at distance d_{sg} from the edge of the wall.

$$\phi_t = \frac{\varepsilon_c}{(c_\theta - d_{sg})} \quad (8)$$

Subtracting the elastic curvature (ϕ_e) from the total curvature (ϕ_t) gives the plastic curvature (ϕ_p) at the given drift level.

$$\phi_p = \phi_t - \phi_e \quad (9)$$

The elastic curvature can be calculated by:

$$\phi_e = \frac{M}{E_c \times I_c} \quad (10)$$

Where, M is the moment at the base of the wall, E_c is the modulus of elasticity of concrete, and I_c is the moment of inertia of the concrete section

Once the plastic curvature was known, the plastic hinge height was calculated as:

$$L_p = \frac{\Delta_t - \Delta_e}{\phi_p \times h_w} \quad (11)$$

Where, Δ_t is the total displacement at the top of the wall, Δ_e is the displacement at the top of the wall due to elastic flexural deformation, and h_w is the height of the wall.

Table 4 shows the comparison of experimentally obtained plastic hinge height with that calculated from equations presented in Table 3. The plastic hinge heights for the experimental walls were calculated at 2% drift. The predictions were relatively accurate in a few of the walls (TW1, TW2, and PreWEC). However, overall, the equations in Table 3 did not predict the plastic hinge height well. The equations given by Kurama (2005)[22] and Aaleti and Sritharan (2009)[23] only consider the wall geometry. The equations by Rahman and Restrepo (2000)[11] and Perez et al. (2004)[4] account for axial compressive force by relating plastic hinge height with neutral axis depth. However, they also did not predict the plastic hinge height well. It should be noted that some of the experimental plastic hinge heights may be outliers due to uncertainty in concrete cracking, variation in location and type of concrete gauges, and properties of concrete/grout used at foundation-wall interface. Sharma and Aaleti (2019)[24] showed that plastic hinge height is dependent upon the amount of axial load imposed on the wall. They developed a linear relationship between the ratio of the plastic

hinge height to the height of the wall and the axial force ratio (AFR). Although their prediction of the plastic hinge height better matches the experimental data compared with ACI ITG 5.2-09 equation, more data are needed to accurately predict the plastic hinge height.

Table 4. Comparison of experimental and analytically predicted plastic hinge heights

Researcher	Specimen	L_p (exp) (in.)	L_p (Rahman & Restrepo) (in.)	L_p (Perez) (in.)	L_p (Kurama) (in.)	L_p (Aaleti & Sritharan) (in.)
Rahman and Restrepo (2000)[11]	Unit 1	21.1	3.83	4.9	10.6	8.7
	Unit 2	89.5	6.16	4.9	10.6	8.7
Perez et al. (2004)[4]	TW1	17.6	20.40	6.0	20.0	17.1
	TW2	26.4	19.40	6.0	20.0	17.1
	TW3	55.3	23.20	6.0	20.0	17.1
	TW4	29.9	17.00	6.0	20.0	17.1
	TW5	44.1	14.70	6.0	20.0	17.1
Sritharan et al. (2015)[18]	PreWEC	12.0	10.90	6.0	14.4	14.4
Liu (2016)[19]	PFS-2	59.7	8.40	6.0	13.6	13.2
Twigden et al. (2017)[13]	SRW-A	12.3	2.80	4.7	7.8	7.4
	SRW-B	35.0	4.70	4.9	6.3	7.1
	PreWEC-B	21.4	4.30	4.9	6.3	7.1

RESIDUAL DRIFT

A subset of the experimental data given in Table 1 was analyzed to evaluate residual drift. The residual drift in rocking walls, hybrid walls and walls with end columns are discussed separately. In the case of rocking walls, residual drift (RD) observed during experiments were mostly below 0.05% (see Table 5). Premature crushing of confined concrete, yielding or rupture of post-tensioning strands result in loss of self-centering ability in rocking walls. However, rocking walls subjected to sufficient axial load may re-center even after total loss of initial PT force (e.g., specimen TW5).

In the case of hybrid walls, there are different guidelines for design of energy dissipating reinforcement to preserve self-centering. ACI ITG-5.1-07[25] (R1.2.3) recommends a 40% cap on moment contribution from energy dissipating reinforcement (M_{ED}), to preserve self-centering following a major seismic event. ACI ITG-5.2-09[2] (5.3.1) recommends a minimum prestress force such that the compressive force exerted by prestressing and additional axial load on the wall is large enough to overcome the maximum tensile force that can develop in the energy-dissipating reinforcement. The minimum prestress force recommended by ACI ITG-5.2-09[2] (5.3.1) is:

$$A_{ps}f_{se} + 0.9D_c = A_s f_u \quad (12)$$

Table 5: Residual drift in rocking walls as obtained by experiments and axial load

Researcher	Specimen ID	Drift (%)	Base Shear (kip)	RD (%)	Average Axial Load (N) kip	Initial Prestress (kip)	Loss in initial prestress (%)
Rehman and Restrepo (2000)[8]	Unit 1	0.9	9	<0.04	3.6	328	6.8
		1.8	11				8.4
		2.7	12				14.2
Perez et al. (2005)[21]	TW2	1.0	145	0.02	173	650	1.0
		1.5	150	0.02			2.3
		2.0	156	0.05			7.9
		3.0	154	0.10			28.9
	TW3	1.0	144	0.03	173	662	1.7
		1.5	153	0.01			2.6
		2.0	151	0.01			10.8
	TW4	1.0	102	0.01	173	332	3.1
		1.5	113	0.01			4.6
		2.0	120	0.01			6.7
		3.0	129	0.03			10.2
	TW5	1.0	92	0.02	173	328	2.7
		2.0	98	0.01			12.2
		3.0	96	0.00			42.4
		4.0	89	0.03			84.6
		5.0	87	0.05			94.6
		6.0	85	0.02			100.0

where $A_{ps}f_{se}$ is the effective prestressing force, D_c is the self-weight of the wall plus any dead loads acting on it, $A_s f_u$ is the tensile strength of all the energy dissipating reinforcement. $\frac{M_{ED}}{M_{wall}}$ ratio (M_{wall} is the moment demand on the wall system) and $\frac{A_{ps}f_{se}+0.9D_c}{A_s f_u}$ is the ratio calculated from the experimental data and tabulated in Table 6. For hybrid walls, M_{ED} was calculated by subtracting moment contribution of post-tensioning force and applied axial load (including self-weight) from M_{wall}.

As seen in Table 6, specimen HW5 exceeded both recommended limits and exhibited a residual drift two times greater than other specimens. Thus, based on the experimental results, it is concluded that limiting moment contribution due to energy dissipating reinforcement below 40% and providing sufficient prestress force to overcome the tensile strength of the energy dissipating reinforcement are adequate in limiting residual drift.

In the case of PreWEC walls, ACI ITG-5.2-09 does not specify a minimum prestress force. However, the residual forces developed in energy dissipating elements of walls with end columns do affect residual drift, albeit in a different way. Unlike in hybrid walls, the energy dissipating elements are on either side of the neutral axis and develop opposing residual forces under cyclic loading. The overturning moment couple created by the residual forces (M_{oED}), if greater than the decompression moment (M_{dec}) causes gap opening at the base of the wall, even after the end of a

seismic event. Thus, M_{oED}/ M_{dec} ratio was calculated at different drift levels along with $\frac{M_{ED}}{M_{wall}}$ ratio and tabulated in Table 7.

Table 6: Residual drift in hybrid walls as obtained by experiments, moment contribution ratios and axial load

Reference	Specimen	Drift (%)	Base Shear (kip)	RD (%)	$\frac{M_{ED}}{M_{wall}}$	$\frac{A_s f_u}{A_{ps} f_{se} + 0.9 D_c}$
Rahman and Restrepo (2000)[11]	Unit 2	1.0	15	<0.12	N/A	0.68
		2.0	17		0.41	
		3.0	18		0.39	
	Unit 3	1.0	24	<0.12	0.40	0.67
		2.0	27		0.41	
		3.0	27		0.40	
Smith (2012)[7], Smith et al. (2010)[8], Smith and Kurama (2014)[17]	HW1	1.1	120	<0.01	0.40	0.75
		1.7	113	0.11	0.40	
		1.9	94	0.12	0.33	
	HW2	1.2	118	<0.12	0.39	0.75
		1.6	114		0.34	
		2.3	103		0.21	
	HW3	1.2	125	<0.01	0.39	0.80
		1.6	125	<0.01	0.37	
		2.3	114	0.18	0.36	
	HW4	1.2	118	<0.16	0.38	0.82
		1.6	120		0.32	
		2.3	118		0.27	
		3.1	112		0.26	
	HW5	1.2	137	0.16	0.62	1.22
		1.6	136	0.28	0.53	
		2.0	140	0.33	0.49	
		2.3	142	0.38	0.48	

As seen in Table 7, the moment contribution from energy dissipating elements was nearly constant at different drift cycles. The $\frac{M_{oED}}{M_{DEC}}$ ratio increased with increasing drift cycles as the residual forces in energy dissipating elements increase and losses in prestressing force accumulated at higher drift. This increment caused greater gap opening at the base of the wall which in turn increased residual drift. Therefore, the design recommendation of limiting moment contribution from energy dissipating members to 40% may not be adequate to ensure self-centering in walls with end columns.

Table 7: Residual drift in walls with end columns and moment contribution ratios

Reference	Specimen	Drift (%)	Base Shear (kip)	RD (%)	$\frac{M_{oED}}{M_{DEC}}$	$\frac{M_{ED}}{M_{wall}}$
Sritharan et al. (2015)[18]	PreWEC-1	1.0	105	<0.11	0.7	0.2
		1.5	110	0.20	0.9	0.2
		2.0	112	0.30	1.0	0.2
		2.5	113	0.44	1.0	0.2
Twigden et al. (2017)[13]	PreWEC-A2	1.0	18	0.11	1.2	0.3
		1.5	19	0.16	1.4	0.3
		2.0	20	0.24	1.5	0.3
		2.5	22	0.28	1.6	0.3
	PreWEC-B	1.0	21	0.18	1.7	0.3
		1.5	23	0.30	2.0	0.3
		2.0	24	0.46	2.3	0.3
		2.5	25	0.56	2.5	0.3
Liu (2016)[19]	PFS-2	1.0	53	<0.1	1.0	0.2
		1.5	56		1.1	0.2
		2.0	58		1.2	0.2

DAMAGE STATES

Precast shear walls experience damage with increasing lateral displacements, albeit much lower than the damage experienced by conventional, cast-in-place walls. In this study, distinct limit states were used to document drifts at which walls in the database went through these distinct states. These limit states were decompression, effective linear limit, cover spalling, yielding of post-tensioning strands, yielding and fracture of energy dissipaters, and crushing of confined concrete. A subset of the database was used for damage classification. Only the studies in which damage observations were sufficiently detailed were used.

Table 8 shows the defined damage states and the drift at which these damage states initiated. Although the number of data points in Table 8 are limited, the following conclusions were drawn. For the specimens given in Table 8, on average, concrete spalling initiated after 1.29% drift, yielding of strands took place after 2.04% drift, yielding of energy dissipaters was after 0.38% drift, concrete crushing occurred after 2.58% drift and energy dissipaters either did not fracture or fractured at 3.0% drift.

Table 8. Damage states and drift ratios associated with each damage state

	Reference	ID	Concrete spalling (%)	Yielding of PT strands (%)	Yielding of energy dissipater (%)	Crushing of confined concrete (%)	Fracture of energy dissipater (%)
Rocking	Perez et al. (2007)[16]	TW1	0.61	1.35	NA	3.57	NA
		TW2	0.65	1.44	NA	2.83	NA
		TW3	0.83	1.63	NA	2.54	NA
		TW4	0.74	2.84	NA	2.97	NA
		TW5	0.65	1.44	NA	NR	NA
	Rahman and Restrepo (2000)[11]	Unit 1	2.80	2.00	NA	NR	NA

Hybrid	Smith (2012)[7], Smith et al. (2010)[8], Smith and Kurama (2014)[17]	HW1	0.40	Not yielded	0.21	1.75	NR
		HW2	0.80	Not yielded	0.21	2.30	NR
		HW3	0.80	Not yielded	0.23	2.30	NR
		HW4	NR	3.00	0.28	3.00	NR
		HW5	NR	2.30	0.35	NR	NR
	Rahman and Restrepo (2000)[11]	Unit 2	2.00	2.00	NR	2.00	3.00
		Unit 3	4.00	2.40	1.00	NR	NR

NA: Not applicable
NR: Not reported

CONCLUSIONS

In this study, a database of precast shear walls tested under quasi-static monotonic or cyclic lateral loading was compiled. First, ACI ITG-5.2-09 provisions on drift and strength capacity of precast shear walls were evaluated by comparing predictions to test results. The average ratio of the drift capacity prediction of ACI ITG-5.2-09 to that of experimental data was 0.58 with a standard deviation of 0.39. Error in predictions is attributed to assumptions made in calculating the plastic hinge height and concrete strain at the extreme fiber. The average ratio of strength as predicted by ACI ITG-5.2-09 to as measured by tests was 0.88, with a standard deviation of 0.23.
The residual displacement was found to be negligible (nearly zero) in rocking walls without any external energy dissipaters. In the case of hybrid walls, ACI ITG-5.2-09 provisions were found to be adequate in limiting residual drift. Additional guidance is needed regarding residual forces in energy dissipating connectors to maintain self-centering in the case of walls with end columns. The plastic hinge height predicted using ACI ITG-5.2-09 and other equations found in the literature did not yield consistent result. Finally, drift ratios at which walls experience changes in behavior (e.g., limit states such as decompression or damage such as cover spalling, strand yielding) were documented for walls in the database.

ACKNOWLEDGEMENTS

This material is based upon work supported by the National Science Foundation under Grant No. 1663063 and 1662963. Any opinions, findings, and conclusions or recommendations expressed in this material are those of the authors and do not necessarily reflect the views of the National Science Foundation.

REFERENCES

1. Priestley MN, Sritharan S, Conley JR, Pampanin S, "Preliminary results and conclusions from the PRESSS five-story precast concrete test building". *PCI J*, 44(6), 1999, 42-67.
2. ACI ITG (American Concrete Institute), "Requirements for design of a special unbonded post-tensioned precast shear wall satisfying ACI ITG-5.1 and commentary", 2009, *ACI ITG-5.2-09,* Farmington Hills, MI.
3. Kurama Y, Sause R, Pessiki S, Lu L-W, "Lateral load behavior and seismic design of unbonded post-tensioned precast concrete walls". *Struct J*, 96(4), 1999, 622-32.

4. Perez FJ, Pessiki S, Sause R, "Lateral load behavior of unbonded post-tensioned precast concrete walls with vertical joints". *PCI J*, 49(2), 2004.
5. Perez FJ, Pessiki S, Sause R, "Experimental Lateral Load Response of Unbonded Post-Tensioned Precast Concrete Walls". *ACI Struct J*, 110(6), 2013.
6. Henry R, "Self-centering precast concrete walls for buildings in regions with low to high seismicity, 2011, University of Auckland, Auckland, New Zealand
7. Smith BJ, "Design, analysis, and experimental evaluation of hybrid precast concrete shear walls for seismic regions, 2012, University of Notre Dame, Notre Dame, Indiana
8. Smith BJ, Kurama YC, McGinnis MJ, "Design and measured behavior of a hybrid precast concrete wall specimen for seismic regions". *J Struct Eng*, 137(10), 2010, 1052-62.
9. Basereh S, Okumus P, Aaleti S, "Reinforced concrete shear walls retrofitted using weakening and self-centering: numerical modeling". *J Struct Eng*, 146(7), 2020, 04020122.
10. Basereh S, Okumus P, Aaleti S, "Seismic retrofit of reinforced concrete shear walls to ensure reparability", Structures Congress 2020, American Society of Civil Engineers Reston, VA.
11. Rahman AM, Restrepo JI, "Earthquake resistant precast concrete buildings: Seismic performance of cantilever walls prestressed using unbonded tendons." Christchurch, New Zeland: University of Canterbury, 2000.
12. Aaleti S, Sritharan S, "Performance verification of the PreWEC concept and development of seismic design guidelines." Ames, Iowa: Iowa State University, 2011.
13. Twigden K, Sritharan S, Henry R, "Cyclic testing of unbonded post-tensioned concrete wall systems with and without supplemental damping". *Eng Struct*, 140, 2017, 406-20.
14. Sritharan S, Aaleti S, Henry RS, Liu KY, Tsai KC, "Precast concrete wall with end columns (PreWEC) for earthquake resistant design". *Earthq Eng Struct D*, 44(12), 2015, 2075-92.
15. Aaleti S, Sritharan S, "A precast wall with end columns (PreWEC) for seismic applications", 8th Pacific Conference on Earthquake Engineering, 2007, Singapore2007.
16. Perez FJ, Sause R, Pessiki S, "Analytical and experimental lateral load behavior of unbonded posttensioned precast concrete walls". *J Struct Eng*, 133(11), 2007, 1531-40.
17. Smith B, Kurama Y, "Seismic design guidelines for solid and perforated hybrid precast concrete shear walls". *PCI J*, 59(3), 2014, 43-59.
18. Sritharan S, Aaleti S, Henry RS, Liu K-Y, Tsai K-C, "Precast concrete wall with end columns (PreWEC) for earthquake resistant design". *Earthq Eng Struct D*, 44(12), 2015, 2075-92.
19. Liu Q, "Study on interaction between rocking-wall system and surrounding structure", 2016, University of Minnesota, Minneapolis, Minnesota.
20. Mander JB, Priestley MJ, Park R, "Theoretical stress-strain model for confined concrete". *J Struct Eng*, 114(8), 1988, 1804-26.
21. Twigden K, Henry R, "Experimental response and design of O-connectors for rocking wall systems". *Structures*, 3, 2015, 261-71.
22. Kurama YC, "Seismic design of partially post-tensioned precast concrete walls". *PCI J*, 50(4), 2005, 100.
23. Aaleti S, Sritharan S, "A simplified analysis method for characterizing unbonded post-tensioned precast wall systems". *Eng Struct*, 31(12), 2009, 2966-75.
24. Sharma S, Aaleti S, "A study on residual drift and concrete strains in unbonded post-tensioned precast rocking walls", Proceedings of the Canadian Conference on Earthquake Engineering, 2019.
25. ACI ITG (American Concrete Institute), "Acceptance criteria for special unbonded post-tensioned precast structural walls based on validation testing", 2007, *ACI ITG-5.1-07*, Farmington Hills, MI.